G. Bernardini, R. Porcelli, J. Serafini, P. Masarati
Rotor Blade Shape Reconstruction from Strain Measurements
Aerospace Science and Technology, Vol. 79, 2018, p. 580-587
doi:10.1016/j.ast.2018.06.012

Rotor Blade Shape Reconstruction from Strain Measurements

Giovanni Bernardini[a], Roberto Porcelli[a], Jacopo Serafini[a], Pierangelo Masarati[b]

[a] *Roma Tre University, Department of Engineering, Via della Vasca Navale, 79, 00144, Roma, Italy*
[b] *Politecnico di Milano, Department of Aerospace Science and Technology, Via Giuseppe La Masa, 34, 20156, Milano, Italy*

Abstract

Traditional helicopter blades are subject to significant deformations, which influence control forces and moments, as well as the helicopter aeroelastic and aeroacoustic behavior. Thus, the knowledge of rotor elastic states could help improving flight control efficiency, and reducing vibration level and acoustic emissions of next-generation helicopters. This paper presents an original and computationally efficient modal approach aimed at dynamic shape sensing of helicopter rotor blades. It is based on strain measurements in a limited number of points over the blade surface. Although the algorithm is based on the cascaded solution of linear algebraic equations, much like other modal-based algorithms, it is able to reconstruct nonlinear, moderate lag, flap and torsional deflections, which are typical in helicopter structural dynamics. The algorithm is tested on non-rotating and rotating hingeless blades through numerical simulations based upon a multibody dynamics solver for general nonlinear comprehensive aeroelastic analysis. Its capabilities are assessed against those of classical modal approaches. Numerical investigations show that the proposed algorithm is reliable, accurate and robust to measurement noise.

Keywords: Helicopter blades, strain gauges, shape sensing

1. Introduction

Rotor blades are subject to significant deformations in standard and critical operating conditions, owing to aerodynamic and inertia loads. They are slender structures, whose flapping deformation, controlled by cyclic pitch, is used to generate rolling and pitching moments and direct rotor thrust. Moreover, it reduces aerodynamic asymmetry between the advancing and retreating sides of the rotor, thus alleviating vibratory loads transmitted to the airframe. Blade shape sensing is a desirable alternative to state observers for Flight Control Systems (FCS) of next-generation helicopters (it is well known that the knowledge of tip-path plane improves the performance of FCS, Refs. 1, 2, 3, 4, 5), as well as for aeroelastic and aeroacoustic control (see for example the Clean Sky GRC5 MANOEUVRES project, which was aimed at demonstrating the possibility to reduce helicopters noise emission in terminal maneuvers through an in-flight monitoring of the main rotor state, Ref. 6).

Although the potential benefits of placing sensors on rotor blades are very clear, two main issues remain open:

(i) the optimal positioning of the sensors on the blade, associated with the risk of accidental breaks during manufacturing or operational life, as well as with the the need to avoid bonding delamination (see Ref. 7 for a complete review of technological issues for the case of sensor application on wind turbines);

(ii) the most efficient way of powering and connecting sensors, in relation with the rotational motion of the rotor.

Both these issues make the use of a large number of sensors more challenging than in fixed wing applications. Following the approach introduced in Refs. 8, 9, 10, in this work the authors propose the use of a limited number of strain gauge measurement points for the real-time determination of the rotor blades shape. Due to both the low cost and reduced weight of the sensors needed to implement such technique, it is easy to foresee its application to a wide range

of rotorcraft, including lightweight helicopters, whose overall performance could be significantly improved.

Although the potential benefits of blade shape sensing are very clear, a viable technological solution to the problem has not yet been identified. Two main classes of shape sensing techniques have been proposed: optical and strain-based. The latter has received more attention in the recent past due to technological and practical problems related to the former. Indeed, while a direct optical measurement (photogrammetry) represents a viable option in some cases (Ref. 11), it may suffer from several disadvantages:

(i) only in-sight parts of objects may be monitored;

(ii) optical markers field of view must be sufficient, i.e. marker plane must form a sufficiently great angle with the direction between camera and marker;

(iii) operating conditions (water, ice, absence of light or direct sun exposure of the camera) make the measurement problematic;

(iv) for real-time, high speed measurements, expensive equipment is required;

(v) camera vibrations heavily affect the accuracy of the measurement.

All these problems are harshly present in rotor blade shape reconstruction, making the application of optical measurements very difficult. On the other hand, shape sensing from strain measurements is an area of growing interest in recent years in many fields of application, ranging from automotive to medical, aerospace and civil engineering. Moreover, Fiber Bragg Gratings strain gauges represent a great improvement in terms of bandwidth and ease of installation with respect to traditional electric resistance solutions. In particular, they drastically reduce the need of cables, as a single fiber may host hundreds of measurement points, whereas each traditional strain gauge needs a dedicated wiring. Their use in rotor blade fatigue monitoring is under investigation (Ref. [12]). Several numerical approaches have been recently proposed for the determination of the deformed shape of bodies from strain measurement; some of them are

based on the direct integration of strain field data at the measurement points (Refs. 13, 14, 15), whereas others use modal expansion, exploiting the use of preliminary FEM analysis on the monitored object (Refs. 16, 17, 18). The latter are usually more efficient in terms of number of required sensors (in the order of tens instead of thousands), but require the knowledge of the object structure. Moreover, with notable exceptions (Ref. 19), the approaches in the literature are inherently linear, whereas in finite strain theory the general relationship between strain and displacement is nonlinear. The modal shape functions may be conveniently evaluated for helicopter rotor blades through an equivalent 1D beam model. However, for linear approaches, rotors may be a challenging application, being subject to moderate deflections in standard operating conditions. Analogous considerations may be drawn for fixed wing aircraft which are becoming more and more flexible.

2. Proposed Approach

In the present work, a modal shape sensing approach is proposed, capable of reconstructing the shape of a beam-like structure subject to general deformations including torsion, in-plane, and out-of-plane bending. It is able of handling nonlinear terms up to second order. This is particularly interesting for flight dynamics and aeroelastic control applications, in which the knowledge of limited information on rotor kinematics may give unsatisfactory results. It is worth mentioning that, at present, devices for the identification of the rotor state (e.g. by measuring cyclic flapping components β_c and β_s, or flapping-related displacement on a point along the blade) are still under development (Ref. 11).

2.1. Strain-displacement relationship

Consider the approximation proposed in Ref. 20 for the strain-displacement relationship of a bent and twisted beam, which is valid for moderate deflections

$$\begin{aligned}\varepsilon_{\xi\xi} = \; & u' + \frac{1}{2}(v'^2 + w'^2) - \lambda\phi'' + (\eta^2 + \zeta^2)\left(\vartheta'\varphi' + \frac{\varphi'^2}{2}\right) \\ & - v''[\eta\cos(\vartheta+\varphi) - \zeta\sin(\vartheta+\varphi)] \\ & - w''[\eta\sin(\vartheta+\varphi) + \zeta\cos(\vartheta+\varphi)]\end{aligned} \tag{1a}$$

$$\varepsilon_{\xi\eta} = -\frac{1}{2}\left(\zeta + \frac{\partial\lambda}{\partial\eta}\right)\varphi' \tag{1b}$$

$$\varepsilon_{\xi\zeta} = \frac{1}{2}\left(\eta - \frac{\partial\lambda}{\partial\zeta}\right)\varphi' \tag{1c}$$

where η and ζ are the coordinates along the cross-section principal axes, ξ is the coordinate along the elastic axis, u, v, and w are the axial, lead-lag and flap displacements of the elastic axis, whereas ϑ and φ are the built-in twist angle and the blade cross-section elastic rotation (torsion), respectively. Note that, in the following, the warping function λ in Eqs. (1) will be neglected for the sake of simplicity. However, its contribution may be easily included if necessary (*e.g.* when the method is applied to composite blades [21, 22]), following one of these approaches:

i) numerically, evaluating the warping function with a finite element (or equivalent) analysis;

ii) experimentally, in a known-displacement calibration test, determining the warping function and its derivatives in the measurement points exploiting strain measurements and the free–contour boundary condition (see Ref. 23);

iii) during the use of the device, using the strain components at the measurement points, and exploiting the fact that in cylindrical portions of the blade the warping function only depends on η and ζ. In this case, it is worth noting that an iterative procedure for the simultaneous evaluation of the unknowns in Eqs. (1a)-(1c) is needed, due to their intrinsic nonlinearity.

In the proposed formulation, the displacement $\boldsymbol{\delta} = \{u, v, w\}^T$ and the elastic torsion angle φ are first expressed as the linear combination of suited shape

functions ($\boldsymbol{\Psi}_i$ and Φ_i), with coefficients q_i and r_i

$$\boldsymbol{\delta}(\xi, t) = \sum_i \boldsymbol{\Psi}_i(\xi)\, q_i(t) \tag{2a}$$

$$\varphi(\xi, t) = \sum_i \Phi_i(\xi)\, r_i(t) \tag{2b}$$

Then, Eqs. (1b) and (1c) are combined into a single equation which gives the shear strain in the direction orthogonal to ξ and tangent to the external surface,

$$\varepsilon_t := t_\eta \varepsilon_{\xi\eta} + t_\zeta \varepsilon_{\xi\zeta} = \frac{-t_\eta \zeta + t_\zeta \eta}{2} \varphi' \tag{3}$$

where t_η, t_ζ are the components of a unit vector lying in the plane of the section, thus with $t_\xi \equiv 0$, and tangent to the surface in the measurement point, or

$$\varepsilon_t = \boldsymbol{k}\boldsymbol{r} \tag{4}$$

where $\boldsymbol{r} = \{r_1, r_2, \ldots, r_M\}^T$ contains the M torsion modal amplitudes, and $\boldsymbol{k}$ is a row vector evaluated in a straightforward manner from the knowledge of the torsion shape functions and the location of the evaluation point. After the torsion amplitudes are obtained from a suitable over-collocation of Eq. (4), Eq. (2b) is used to calculate the terms that depend on φ in Eq. (1a), leaving the displacement components as the only unknowns.

Finally, evaluating Eq. (1a) at two points of the same cross-section, and subtracting the corresponding $\varepsilon_{\xi\xi}$ values, one obtains

$$\begin{aligned}
\Delta\varepsilon_{\xi\xi} &= \varepsilon_{\xi\xi_2} - \varepsilon_{\xi\xi_1} \\
&= \left[\left(\eta_2^2 + \zeta_2^2\right) - \left(\eta_1^2 + \zeta_1^2\right)\right] \left(\vartheta'\varphi' + \frac{\varphi'^2}{2}\right) \\
&- v'' \left[(\eta_2 - \eta_1)\cos(\vartheta + \varphi) - (\zeta_2 - \zeta_1)\sin(\vartheta + \varphi)\right] \\
&- w'' \left[(\eta_2 - \eta_1)\sin(\vartheta + \varphi) + (\zeta_2 - \zeta_1)\cos(\vartheta + \varphi)\right]
\end{aligned} \tag{5}$$

where subscripts 1 and 2 refer to two measures at the same radial station ξ. Using N shape functions to approximate $\boldsymbol{\delta}$, Eq. (5) is a purely linear relationship between the difference $\Delta\varepsilon_{\xi\xi}$ and $\boldsymbol{q} = \{q_1, q_2, \ldots, q_N\}^T$, i.e.

$$\Delta\varepsilon_{\xi\xi} = \boldsymbol{h}\boldsymbol{q} + b \tag{6}$$

where $\boldsymbol{h}$ is a row vector depending on the displacement shape functions, $\boldsymbol{\Psi}_i$, the torsion angle, φ, and the location of the evaluation points, whereas b depends on the torsion angle and the location of the evaluation points, i.e. both $\boldsymbol{h}$ and b depend on the elastic torsion angle, φ, thus making $\Delta\varepsilon_{\xi\xi}$ still potentially nonlinear.

It is worth noticing that, using $\Delta\varepsilon_{\xi\xi}$ (Eq. (6)), instead of $\varepsilon_{\xi\xi}$ (Eq. (1a)) for the evaluation of the elastic axis displacement, the contribution of the axial displacement u vanishes, thus reducing the number of total modes required for blade shape reconstruction when flap and lead-lag are the only linear displacements of interest.

2.2. Torsion and displacement amplitude identification

In order to identify torsion and displacement amplitude from Eqs. (4) and (6), $N + M$ linearly independent equations are needed. The N measurements for $\Delta\varepsilon_{\xi\xi}$ are easily obtained by aligning the sensors with the blade span. The M equations for torsion identification can be obtained by using a set of sensors glued over the blade surface, and oriented at angles α_i with respect to the ξ-axis, their outputs $\varepsilon_{\alpha_i\alpha_i}$ over each cross-section. Indeed, from the strain tensor associated with the Euler-Bernoulli beam

$$\boldsymbol{T} = \begin{bmatrix} \varepsilon_{\xi\xi} & \varepsilon_{\xi\eta} & \varepsilon_{\xi\zeta} \\ \varepsilon_{\xi\eta} & -\nu\varepsilon_{\xi\xi} & 0 \\ \varepsilon_{\xi\zeta} & 0 & -\nu\varepsilon_{\xi\xi} \end{bmatrix}$$

the local strain along a direction tangent to the beam surface, identified by the unit vector $\boldsymbol{m}$ (see Fig. 1), is given by

$$\varepsilon_{mm} = (\boldsymbol{T}\boldsymbol{m}) \cdot \boldsymbol{m} = [(1+\nu)m_\xi^2 - \nu]\varepsilon_{\xi\xi} + 2m_\xi m_\eta \varepsilon_{\xi\eta} + 2m_\xi m_\zeta \varepsilon_{\xi\zeta} \qquad (7)$$

where $\{m_\xi, m_\eta, m_\zeta\}$ are the components of the unit vector $\boldsymbol{m}$. Notice that, being the twist of a helicopter blade relatively small, the optimal sensor orientation to eliminate the contribution of the axial strain, $\varepsilon_{\xi\xi}$, from the difference of the signals of two sensors located at the same measurement point is $\alpha_i \approx \pm 45°$.

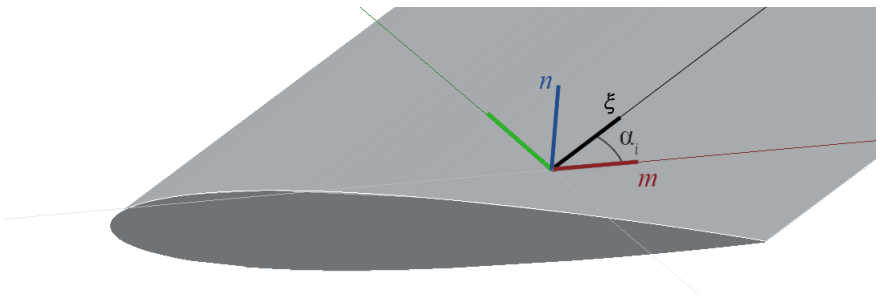

Figure 1: Sensor orientation.

These equations can be obtained by performing N measurements for $\varepsilon_{\xi\eta}$ and $\varepsilon_{\xi\zeta}$, and M measurements for $\Delta\varepsilon_{\xi\xi}$ at different cross-sections along the blade span, which implies at least an additional measure for each spanwise station that is considered. Note that the sections used for torsion and displacement identification may coincide and, in this case, one of the measurements used for $\Delta\varepsilon_{\xi\xi}$ on each section may be conveniently replaced with the weighted sum of the signals from the two $\pm 45°$ sensors. Thus, the minimum number of sensor on each instrumented section is three. However, owing to the presence of noise and measurement errors in both signal acquisition/processing and sensor positioning processes, a greater number of measurements are required to obtain a reliable evaluation of the modal amplitudes.

Formally, the proposed solution procedure can be written as

$$\min_{\boldsymbol{r},\boldsymbol{q}} J = \boldsymbol{e}_t^T \mathbf{W}_t \boldsymbol{e}_t + \boldsymbol{e}_b^T \mathbf{W}_b \boldsymbol{e}_b \tag{8}$$

where $\mathbf{W}_t$ and $\mathbf{W}_b$ are symmetric, positive definite torsion (subscript t) and bending (subscript b) weight matrices, and $\boldsymbol{e}_t$ and $\boldsymbol{e}_b$ are the corresponding error measures, defined as

$$\boldsymbol{e}_t = \mathbf{K}\boldsymbol{r} - \boldsymbol{\varepsilon}_t \tag{9a}$$

$$\boldsymbol{e}_b = \mathbf{H}\boldsymbol{q} + \boldsymbol{b} - \Delta\boldsymbol{\varepsilon}_{\xi\xi} \tag{9b}$$

where matrices $\mathbf{K}$ and $\mathbf{H}$ are obtained by stacking the rows $\boldsymbol{k}$ and $\boldsymbol{h}$ of Eqs. (4) and (6), respectively, for each sensor. Recall that the elements of vector $\boldsymbol{b}$ in

the bending error of Eq. (9b) may depend on the torsional solution $\boldsymbol{r}$, so the function that needs to be minimized is not purely quadratical in the unknowns $\boldsymbol{r}$ and $\boldsymbol{q}$.

For both torsion and bending, the problem becomes linear by solving it with $\mathbf{W}_t = \mathbf{I}$ and $\mathbf{W}_b = \mathbf{0}$ first, and then, after evaluating $\boldsymbol{b}$ with the values of $\boldsymbol{r}$ resulting from this first step, by repeating the minimization with $\mathbf{W}_t = \mathbf{0}$ and $\mathbf{W}_b = \mathbf{I}$.

Alternatively, a weighting of $\mathbf{W}_t = w_t\mathbf{I}$ and $\mathbf{W}_b = w_b\mathbf{I}$ can be assumed, with w_t and w_b positive scalars, considering the limit for $w_t/w_b \to \infty$, a choice that privileges the torsion solution over the bending one.

The separate overdetermined problems can thus be solved in a staggered manner as

$$\boldsymbol{r} = \mathbf{K}^{+}\boldsymbol{\varepsilon}_t \tag{10}$$

and, after evaluating b using the torsion angle resulting from $\boldsymbol{r}$,

$$\boldsymbol{q} = \mathbf{H}^{+}(\Delta\boldsymbol{\varepsilon}_{\xi\xi} - \boldsymbol{b}) \tag{11}$$

where $(\cdot)^{+}$ indicates the Moore-Penrose pseudo-inverse.

Notice that the evaluation of $\Delta\varepsilon_{\xi\xi}$ requires one additional strain gauge per each spanwise station, with an increase of sensors with respect to those used in classical modal approaches (see for example Ref. 17), which are equal to the number of modes. This drawback is largely compensated by the fact that the proposed procedure is computationally very efficient, as it allows one to solve nonlinear elasticity problems (under the assumption that bodies are subject to moderate deformations) through the sequential solution of two linear algebraic systems (Eqs. (10) and (11)). Furthermore, it appears to be quite accurate since, due to error propagation, a single measurement of $\Delta\varepsilon_{\xi\xi}$ is statistically more precise than one of $\varepsilon_{\xi\xi}$.

3. Numerical Results

The test cases considered in this section refer to hingeless rotor blades whose equivalent structural properties resemble those of the Bölkow (now Airbus Helicopters) BO105 helicopter blades, with a radius of 4.9 m rotating at 44.4 rad/s, either in hover or in forward-flight at an advance ratio of $\mu = 0.2$. The first blade model analyzed is uniform, whereas the second one is strongly non-uniform, having a maximum variation of the bending stiffness of about 24000 %. Figure 2 illustrates the qualitative trend of the main structural properties along the blade (note that, in the second plot, the one related to the flap and lag stiffness properties, the y-axis scale is logarithmic). The uniform blade structural properties are equal to those at the tip of the non-uniform one.

The actual measurements on the surface of rotor blades are simulated using the elastic axis shape numerically computed by means of dynamic and aeroelastic simulations performed with the free, general purpose multibody dynamics solver MBDyn (Ref. 24), and hypothesizing a NACA0012 profile.

3.1. Static results

The first analysis performed is the flap-wise bending reconstruction of the non-rotating blade. In Fig. 3, the results of the proposed approach are compared with those of the linearized model for small displacements.

Unless otherwise stated, here and in the following, two pairs of $\pm 45^\circ$ sensors over the same section are considered ("measurement section", in the following) for both blade upper and lower surfaces. Notice that this is not an optimal sensor arrangement, which would require a dedicated analysis. Some authors (Ref. 25) have proposed the use of the condition number (CN) of matrices $\mathbf{H}$ and $\mathbf{K}$ as an estimate of the quality of sensor placement. In addition, it should be noticed that optimal positioning should also take into account the expected value of the measurement, to improve the signal to noise ratio.

Two and three bending modes are respectively used for the definition of the $\mathbf{H}$ and $\mathbf{K}$ matrices in Eqs. (10) and (11) (homogeneous beam modes are considered). Since the aim was to investigate the difference in terms of accuracy of the

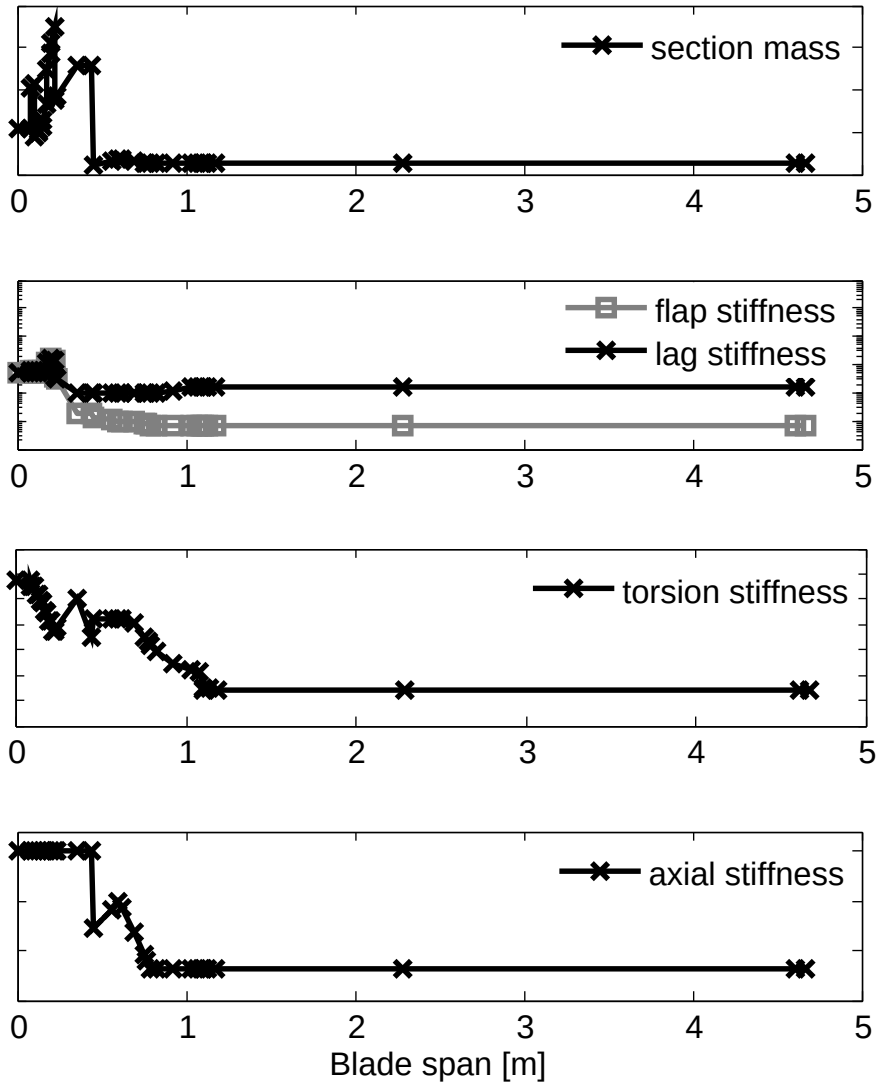

Figure 2: Structural properties along blade.

185 proposed approach *versus* the classical modal approaches, the number of measurement sections has been set relatively high (six sections), in order to consider results close to convergence. In this case, the proposed formulation is equivalent to the classic modal approach to shape sensing, as expected, since the nonlinear terms are negligible. Analogous results (not shown here, for conciseness) have

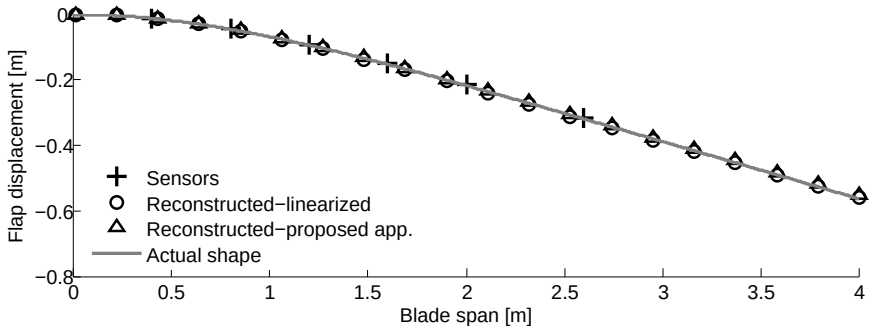

Figure 3: Shape reconstruction for a small-displacement flap bending. Comparison between linearized and proposed approach.

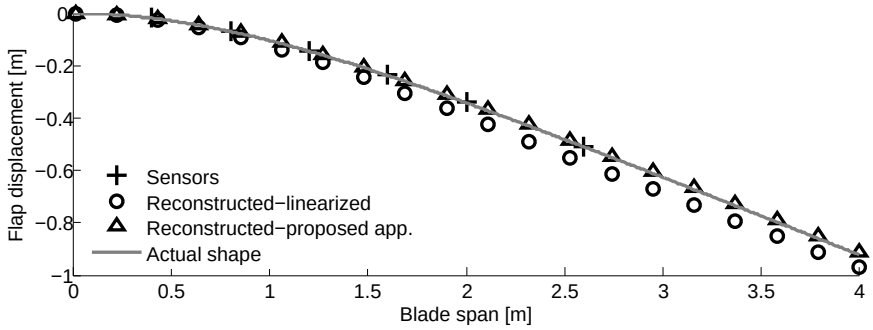

Figure 4: Shape reconstruction for a moderate-displacement flap bending. Comparison between linearized and proposed approach.

been obtained for the lag deformation. On the contrary, when displacements become larger, the effect of the nonlinear terms is no longer negligible. In this case, illustrated in Fig. 4, the proposed approach provides a much more accurate shape reconstruction.

Figure 5 shows the reconstruction of the torsion deformation of the same blade. Here, eight measurement sections were required to obtain results close to convergence. Only the result from the proposed approach is shown, since the torsion problem stated in Eqs. (1b) and (1c) is linear.

Sensitivity to sensors positioning.

Figures 6 and 7 depict the effect of the spanwise position of the sensors, both

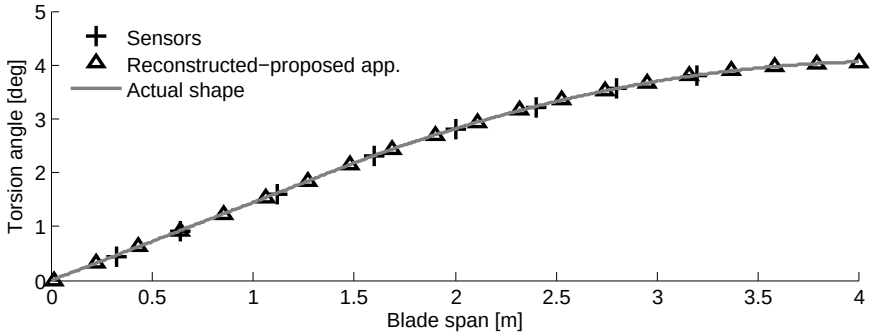

Figure 5: Shape reconstruction for a torsion-forced beam.

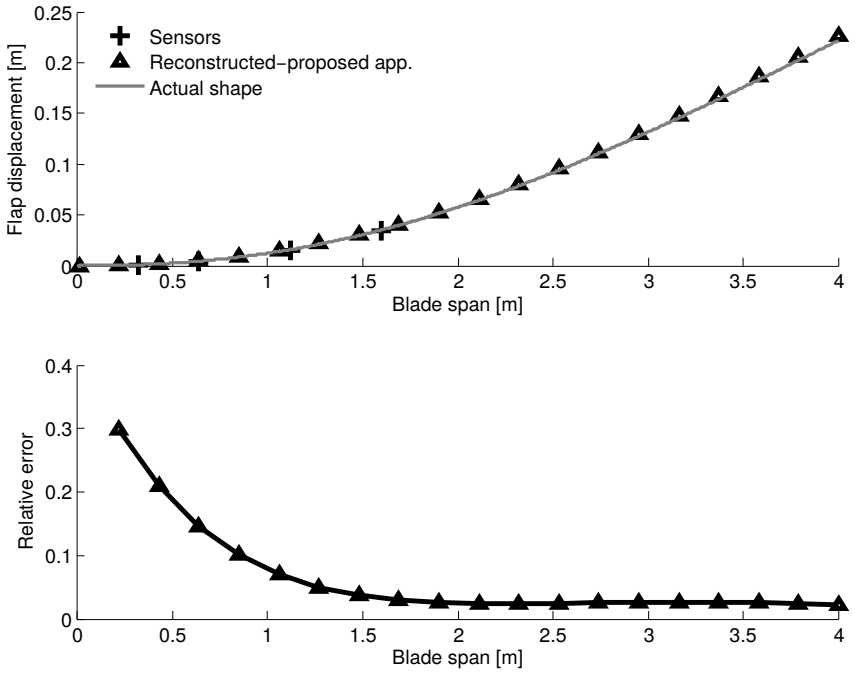

Figure 6: Flap reconstruction using sensors near the blade root.

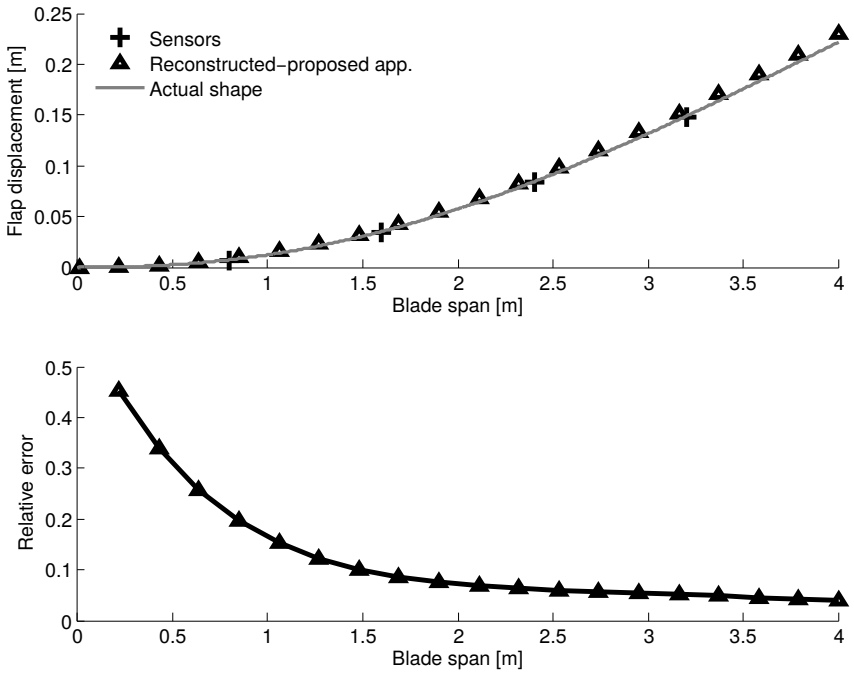

Figure 7: Flap reconstruction using sensors uniformly distributed along the blade.

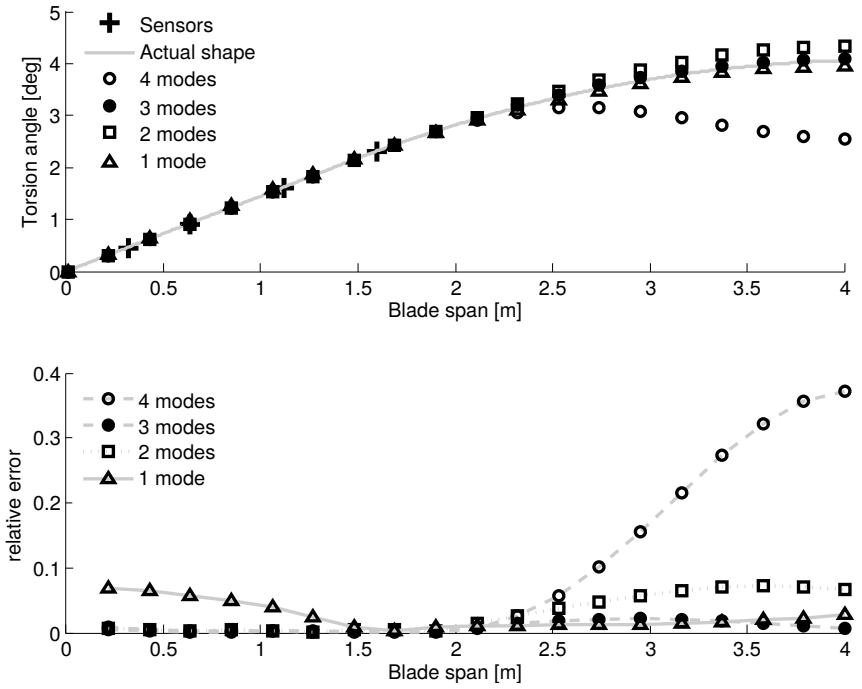

Figure 8: Torsion reconstruction varying number of modes.

in terms of flapwise bending reconstruction and relative error. In Figure 6, four sensors are clustered near the blade root section, whereas in Figure 7 the same number of sensors are uniformly distributed over the whole span. As expected, placing the sensors closer to the root, where the strains associated with low-frequency modes are usually larger, reduces the reconstruction error. Figure 6 also shows that the error may be made sufficiently small for helicopter blade shape sensing with a reduced number of sensors.

Sensitivity to modal base.

Figure 8 presents a sensitivity analysis with respect to the number of modes used in the reconstruction algorithm. It depicts the torsion deformation obtained by increasing the number of the torsion modes, and using the four instrumented sections clustered near the blade root. Expanding the modal base up to three modes gives an improvement of the reconstruction quality, whereas the use of

Table 1: Condition number of **H** and **K** matrices for different bending and torsion modes number (four sections, three total sensors per section).

	1	2	3	4
H	1	15.82	9.80e02	2.61e05
K	78.74	1.59e03	6.53e02	8.60e06

four modes seems to produce a dramatic worsening of the accuracy. The same analysis performed on flap and lead-lag deformations (not presented here for the sake of conciseness) shows that the optimal number of modes is two, although the sensitivity of the reconstruction accuracy to the modes number is less pronounced. The negative effect of increasing the number of modes fixing the number of sensors can be also inferred by Table 1, which reports the condition number of the **H** and **K** matrices when the modes number is varied. Here the number of sensors per section has been kept to a minimum, which is equal to three, assuming that two sensors are used for evaluating torsion and bending at the same time (subtracting and adding their signals appropriately). Globally, the modes increase results in a degradation of the matrices conditioning, which become ill-conditioned when four modes are used. It is worth recalling that the reconstruction accuracy is a trade-off between a well-conditioned system and an appropriate number of modes (see Fig. 9). If a high number of modes is required due to the nature of the problem, a simultaneous increase of the number of sensors is needed, taking care to position them in a suited way to keep the condition number low.

Thus far, a homogeneous blade has been considered. In other words, the modal base used for the definition of the **H** and **K** matrices of Eqs. (10) and (11) is the proper base for the problem examined. If we consider a non-uniform blade in the simulation, the overall quality of the shape reconstruction decreases significantly, for the same number and type of modes, also considering a high number of measurement sections (Figs. 10 and 11).

However, using non-uniform blade modes, the reconstruction accuracy is restored, as shown in Figs. 12 and 13. Since for real-life applications a reasonably

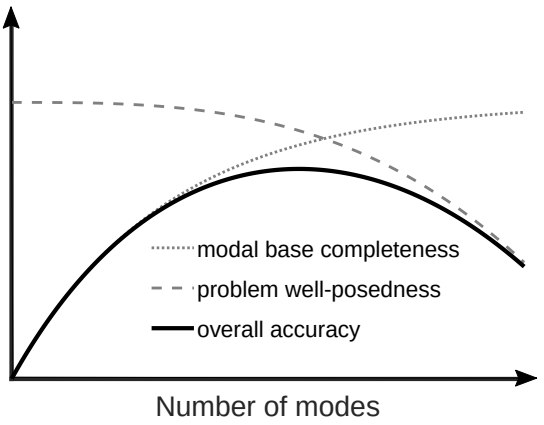

Figure 9: Opposite consequence of increasing the number of modes on shape sensing accuracy.

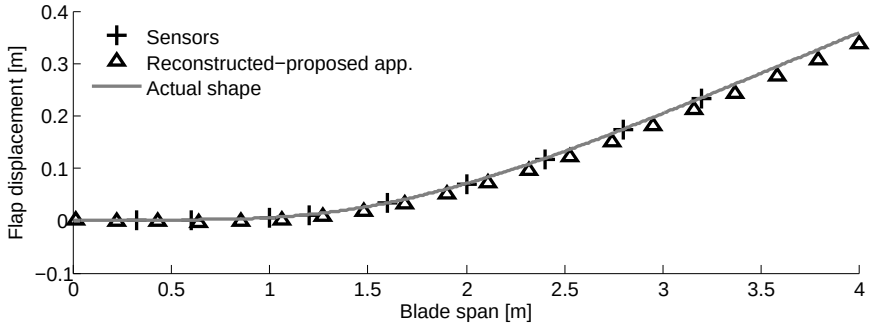

Figure 10: Shape reconstruction of a non-uniform blade, using modes of a uniform one.

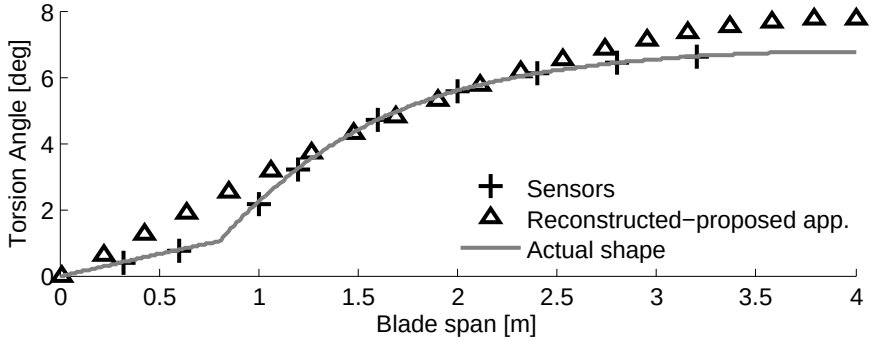

Figure 11: Shape reconstruction of a non-uniform blade, using modes of a uniform one.

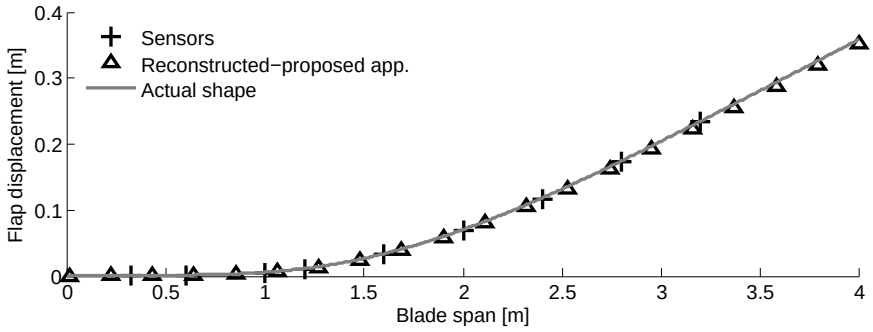

Figure 12: Shape reconstruction of a non-uniform blade, using its natural modes.

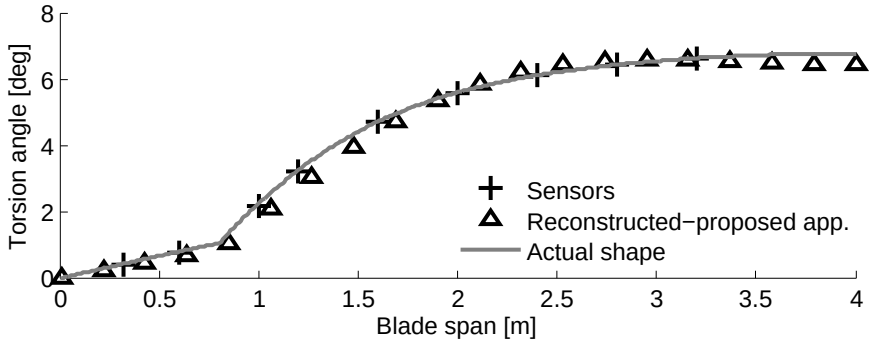

Figure 13: Shape reconstruction of a non-uniform blade, using its natural modes.

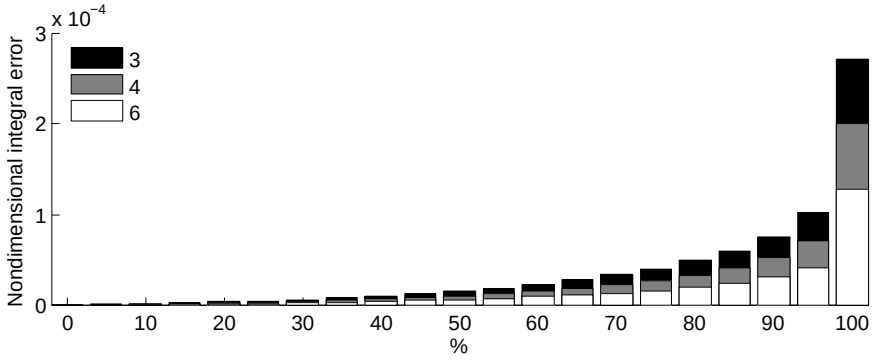

Figure 14: Ventiles of error for different number of sensors over each measurement section.

accurate FEM model of the blade is usually available, the evaluation of its eigenmodes, or their experimental determination [26, 27], is a convenient operation, which reduces the number of modes that need to be considered (and thus of sensors to be installed).

Sensitivity to measurement noise.

Another issue that is addressed here is the influence of measurement noise on the robustness of the result. In particular, the effect of redundant measurement sections on disturbance rejection has been investigated. Considering a random noise equal to 0.2×10^{-6} plus 10% of the measurement (which is a value significantly higher than that expected for a modern strain sensor), the reconstruction error for a flap bending case has been evaluated over ten thousand simulations with different numbers of couples of $\pm 45°$ sensors (3,4,6) for each measurement section. Fig. 14 shows the resulting ventiles of integral error (namely $\frac{1}{L^3}\int_0^L \left(w_r - w_s\right)^2 dx$). It appears clearly that by increasing the number of sensors, the error is significantly reduced.

3.2. Dynamical results

Figure 15 shows the tip-flap displacement for a periodically forced, yet non-rotating case. Figure 16 reports the tip displacement components for the rotating blade. In this case, one lag mode, four flap modes and two torsion modes are used in the reconstruction, which uses six measurement sections. As

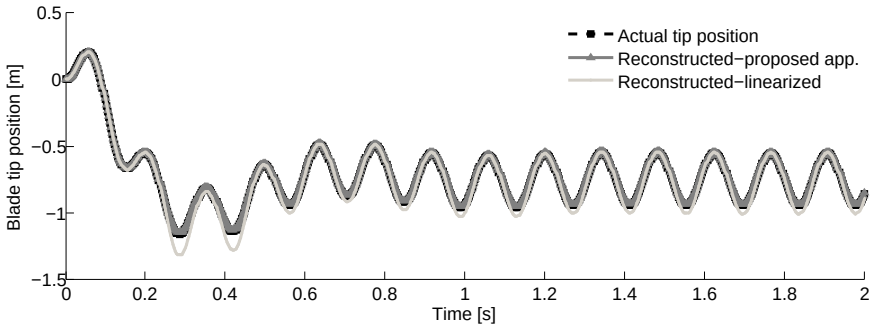

Figure 15: Time history of actual flap displacement of tip and its reconstruction with linearized and proposed approach.

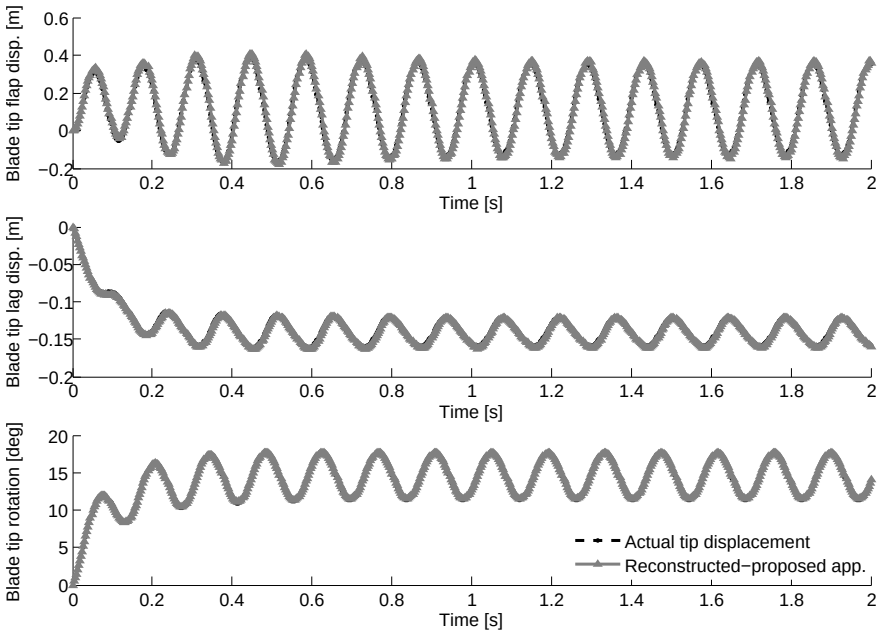

Figure 16: Reconstruction of tip flap, lag and torsion displacements of the rotating blade.

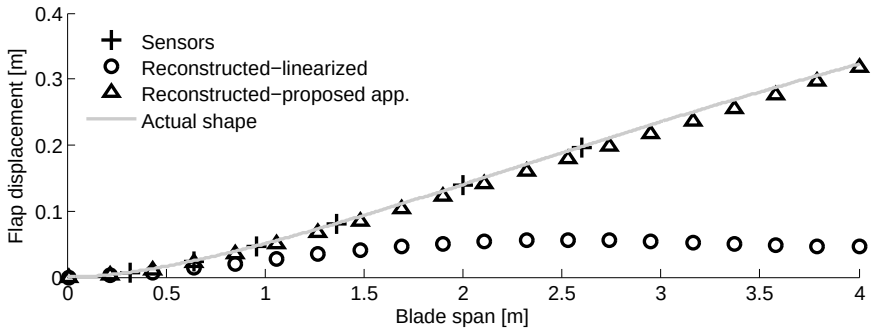

Figure 17: Shape reconstruction of a rotating blade. The linearized approach is here applied without including axial modes.

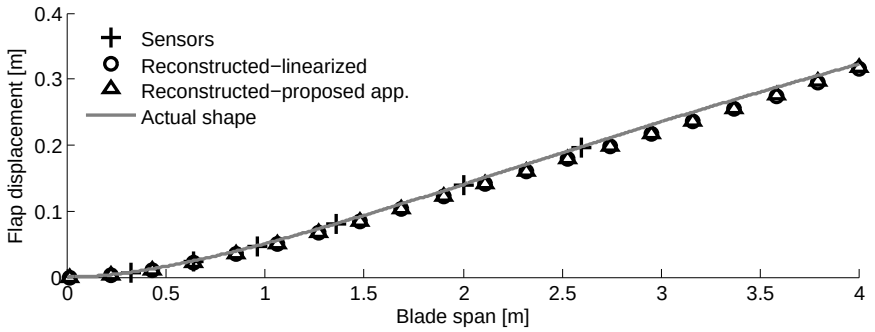

Figure 18: Comparison between proposed approach and linearized one (including axial mode) for a rotating case.

stated in Section "Shape Sensing Algorithm", axial modes are not needed for the proposed approach. On the contrary, with the linearized approach it is strictly necessary to introduce them, since a significant part of strain is due to the centrifugal force field. Figure 17 shows what happens when no axial modes are included in the simulation for the linearized approach. In this case, after introducing a single axial mode, the quality of the reconstruction is restored, as shown in Fig. 18. However, this comes at the cost of an increase of modes that need to be evaluated and thus of the number of required sensors.

Figure 19 shows the time history of the integral error (defined as above)

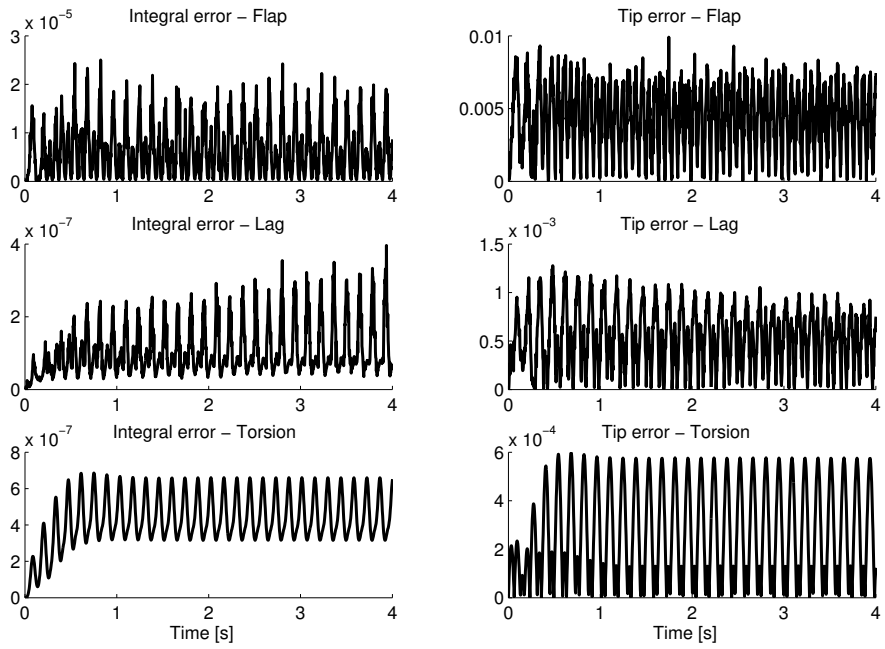

Figure 19: Integral and tip error using one lag, four flap and two torsion modes, considering four instrumented sections.

and the relative error at the blade tip. Although quite small, the error on flap displacement is significantly larger than those on lag and torsion. Increasing the number of instrumented sections and modes from four to eight (Figure 20) significantly improves the shape reconstruction. Note that increasing the number of sensors requires a corresponding increase of the instrumented portion of the blade, to maintain a small conditioning number for both the $\mathbf{H}$ and $\mathbf{K}$ matrices. This caution is needed, since natural modes behave similarly in the vicinity of the blade root.

Notice that a reduction of required modes may also be achieved by considering those of a rotating beam.

3.3. Application to complex structures

It is worth mentioning that the proposed approach could be also applied to subparts (beams) of complex structures. This makes it possible to retain also

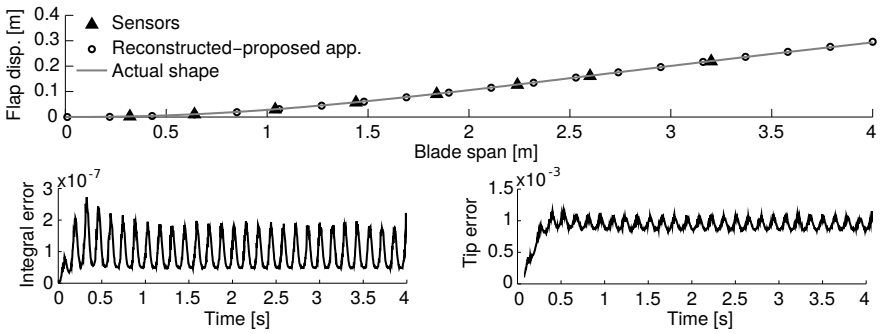

Figure 20: Integral and tip error on flap using eight flap modes, considering eight instrumented sections.

the evaluation of second order terms in cases where the analytical relationship between displacement and strain is unknown. The drawback is that for the evaluation of the structure's global shape a post-processor is needed, which enforces compatibility of the subparts' deformation.

Here, with the aim of assessing the effectiveness of the shape sensing procedure on complex 3D structures, composed of different structural elements (*e.g.,* 3D elements, beams and shells), the wing box sketched in Figure 21 has been considered. For this analysis, an approximate distribution of the aerodynamic loads is considered, linearly varying along the wing chord and elliptically varying along the wing span.[28] Nine virtual strain gauges are positioned on the upper skin, in the first third of the wing span from the root (see Figure 21). Results in terms of spanwise distribution of the out-of-plane displacement are shown in Figure 22, where results from a FEM analysis are compared with the reconstruction obtained using two modes. Note that in this case the accuracy of the reconstruction algorithm is weakly dependent on the number of modes. Indeed, a similar analysis, performed using only one mode for the out-of-plane displacement reconstruction, provided results with less than 1% error at the wing tip.

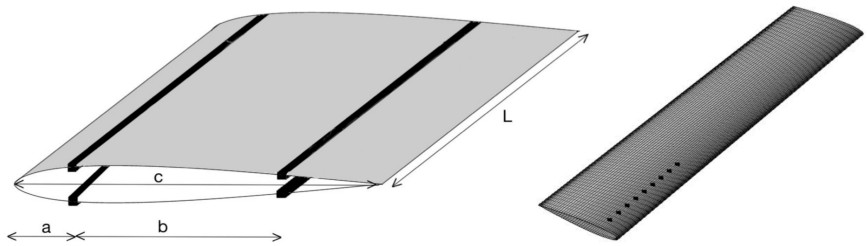

Figure 21: Idealized wing structure (C=1 m, L=6.5 m, a=0.22 m, b=0.57 m). Black dots on the right picture represent measurement points location.

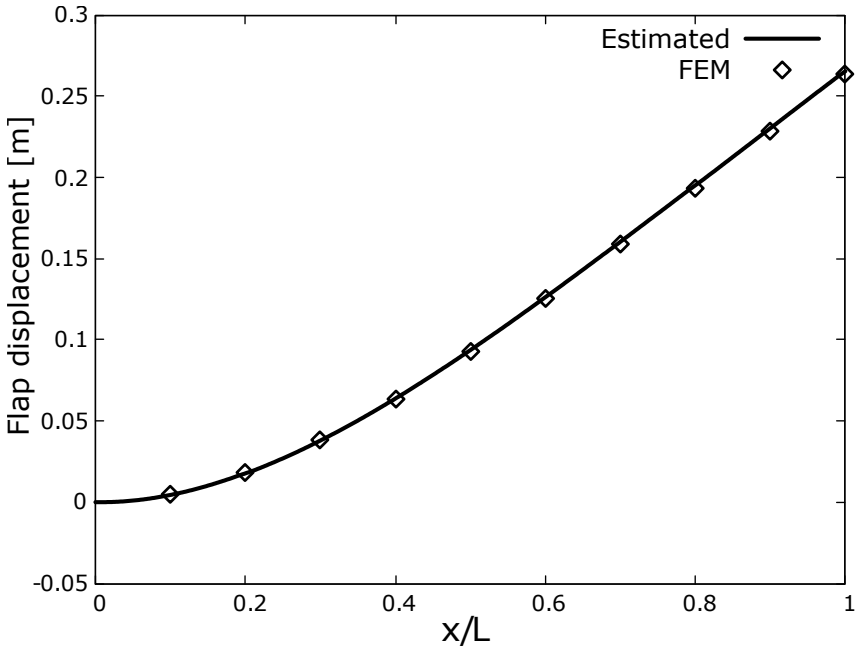

Figure 22: Simulated and reconstructed wing deflection.

4. Conclusions

The numerical testing of the shape sensing procedure has given good results in terms of accuracy and precision, with a small number of required strain sensors. In the end, the reconstruction error could be reduced to within a few percent, even using quite a limited number of modes (2 for the flapwise displacement and 3 for the twist) and sensors (4 sections, each with 3 strain gauges). Increasing the number of instrumented sections makes it possible to use a larger modal base, thus reducing the reconstruction error, whereas adding more sensors on each section helps reducing the effect of measurement noise. Having more instrumented sections and more strain gauges on each section would also help dealing with some types of sensor malfunctions. The procedure has also demonstrated its capability to reconstruct the shape of moderately deflected beams (whereas classical modal approaches to shape sensing are limited to small displacements), although the algorithm only requires the solution of linear problems. The determination of the optimal placement of sensors, the capability of dealing with finite displacements and the extension of the algorithm to other seminal structures (*e.g.* plates, shells) are still open issues that will be the subject of future analyses.

Another field of future study is the application of the proposed procedure to complex structures. In this case, it will be necessary to make congruent information from the shape sensing across subparts of the structure.

[1] W. Hall Jr, A. Bryson Jr, Inclusion of rotor dynamics in controller design for helicopters, Journal of Aircraft 10 (4) (1973) 200–206.

[2] M. D. Takahashi, Rotor-state feedback in the design of flight control laws for a hovering helicopter, Journal of the American Helicopter Society 39 (1) (1994) 50–62.

[3] J. F. Horn, W. Guo, G. T. Ozdemir, Use of rotor state feedback to improve closed-loop stability and handling qualities, Journal of the American Helicopter Society 57 (2) (2012) 1–10.

[4] S. Panza, M. Lovera, Rotor state feedback in the design of rotorcraft attitude control laws, in: Advances in Aerospace Guidance, Navigation and Control, Springer, 2015, pp. 205–225.

[5] H. Ji, R. Chen, P. Li, Rotor-state feedback control design to improve helicopter turbulence alleviation in hover, Proceedings of the Institution of Mechanical Engineers, Part G: Journal of Aerospace Engineering 232 (1) (2018) 156–168.

[6] L. Trainelli, M. Gennaretti, G. Bernardini, A. Rolando, C. E. Riboldi, M. Redaelli, L. Riviello, A. Scandroglio, Innovative helicopter in-flight noise monitoring systems enabled by rotor-state measurements, Noise Mapping 3 (1).

[7] S.-W. Kim, W.-R. Kang, M.-S. Jeong, I. Lee, I.-B. Kwon, Deflection estimation of a wind turbine blade using FBG sensors embedded in the blade bonding line, Smart Materials and Structures 22 (12) (2013) 125004.

[8] C. Enei, G. Bernardini, J. Serafini, L. Mattioni, C. Ficuciello, V. Vezzari, Photogrammetric detection technique for rotor blades structural characterization, in: Journal of Physics: Conference Series, Vol. 658, IOP Publishing, 2015, p. 012003.

[9] G. Bernardini, J. Serafini, C. Enei, L. Mattioni, C. Ficuciello, V. Vezzari, Structural characterization of rotor blades through photogrammetry, Measurement Science and Technology 27 (6) (2016) 065401.

[10] G. Bernardini, R. Porcelli, J. Serafini, P. Masarati, Shape sensing and structural health monitoring of rotor blades from strain analysis, in: AHS 73rd Annual Forum, Fort Worth, TX, USA, 2017.

[11] L. Trainelli, M. Gennaretti, E. Zappa, M. Lovera, A. Rolando, P. Cordisco, R. Grassetti, M. Redaelli, Development and testing of innovative solutions for helicopter in-flight noise monitoring and enhanced control based on

rotor state measurements, in: Proceedings of 42nd European Rotorcraft Forum, Lille, France, 2016.

[12] M. Hajek, S. Manner, S. Sußе, Blade root integrated fibre bragg grating sensors - a highly redundant data source for future HUMS, in: AHS 71st Annual Forum and Technology Display, Virginia Beach, VA, 2015.

[13] G. C. Kirby III, T. W. Lim, R. Weber, A. Bosse, C. Povich, S. Fisher, Strain-based shape estimation algorithms for a cantilever beam, in: Smart Structures and Materials' 97, International Society for Optics and Photonics, 1997, pp. 788–798.

[14] C. V. Jutte, W. L. Ko, C. A. Stephens, J. A. Bakalyar, W. L. Richards, Deformed shape calculation of a full-scale wing using fiber optic strain data from a ground loads test, Tech. Rep. TP-2011-215975, NASA (2011).

[15] R. Glaser, V. Caccese, M. Shahinpoor, Shape monitoring of a beam structure from measured strain or curvature, Experimental mechanics 52 (6) (2012) 591–606.

[16] G. Foss, E. Haugse, Using modal test results to develop strain to displacement transformations, in: Proceedings of the 13th international modal analysis conference, Vol. 2460, 1995, p. 112.

[17] P. B. Bogert, E. Haugse, R. E. Gehrki, Structural shape identification from experimental strains using a modal transformation technique, in: Proceedings of 44th AIAA/ASME/ASCE/AHS Structures, Structural Dynamics and Materials Conference, Norfolk, Virginia, 2003.

[18] C.-g. Pak, Wing shape sensing from measured strain, AIAA Journal 54 (3) (2016) 1068–1077.

[19] M. Alioli, P. Masarati, M. Morandini, T. Carpenter, N. B. Osterberg, R. Albertani, Membrane shape and load reconstruction from measurements using inverse finite element analysis, AIAA Journal 55 (1) (2017) 297–308, doi:10.2514/1.J055123.

[20] D. H. Hodges, E. H. Dowell, Nonlinear equation for the elastic bending and torsion of twisted nonuniform rotor blades, Tech. Rep. TN D-7818, NASA (1974).

[21] S. N. Jung, V. Nagaraj, I. Chopra, Assessment of composite rotor blade modeling techniques, Journal of the American Helicopter Society 44 (3) (1999) 188–205.

[22] S. N. Jung, V. Nagaraj, I. Chopra, Refined structural model for thin-and thick-walled composite rotor blades, AIAA journal 40 (1) (2002) 105–116.

[23] H. D. Curtis, Fundamentals of aircraft structural analysis, Richard d Irwin, 1997.

[24] P. Masarati, M. Morandini, P. Mantegazza, An efficient formulation for general-purpose multibody/multiphysics analysis, J. of Computational and Nonlinear Dynamics 9 (4) (2014) 041001, doi:10.1115/1.4025628.

[25] C.-J. Li, A. G. Ulsoy, High-precision measurement of tool-tip displacement using strain gauges in precision flexible line boring, Mechanical Systems and Signal Processing 13 (4) (1999) 531–546.

[26] I. Bucher, D. Ewins, Modal analysis and testing of rotating structures, Philosophical Transactions of the Royal Society of London A: Mathematical, Physical and Engineering Sciences 359 (1778) (2001) 61–96.

[27] B. Peeters, H. Van der Auweraer, et al., Polymax: a revolution in operational modal analysis, in: 1st International Operational Modal Analysis Conference, Copenhagen, Denmark, Apr, 2005, pp. 26–27.

[28] D. P. Raymer, Aircraft Design: A Conceptual Approach and Rds-student, Software for Aircraft Design, Sizing, and Performance Set (AIAA Education), AIAA (American Institute of Aeronautics & Astronautics), 2006.